ACS APPLIED MATERIALS & INTERFACES

Research Article

www.acsami.org

Recyclable Graphene Oxide-Supported Titanium Dioxide Photocatalysts with Tunable Properties

Stuart Linley,[†] YingYing Liu,[‡] Carol J. Ptacek,[‡,§] David W. Blowes,[‡,§] and Frank X. Gu*[,†,∥]

[†]Department of Chemical Engineering, [‡]Department of Earth and Environmental Sciences, [§]The Water Institute, and [∥]Waterloo Institute for Nanotechnology, University of Waterloo, Waterloo, Ontario, Canada

Supporting Information

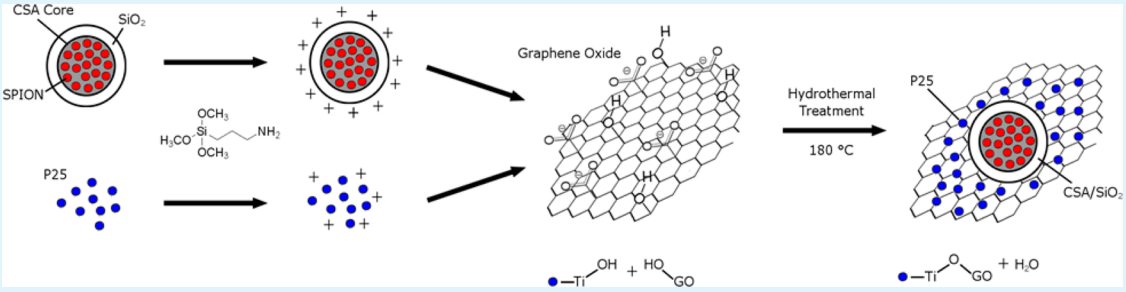

ABSTRACT: A modular synthesis technique was developed for producing graphene-supported titanium dioxide photocatalysts. The modular synthesis allowed for simple tuning of the ratio of particle loading on the graphene oxide (GO) surface as well as good photocatalytic activity of the composite and quick, efficient magnetic separability. GO flakes were used as a support for titanium dioxide nanoparticles and SiO_2 insulated nano-sized magnetite aggregates. Different composition ratios were tested, resulting in a catalyst formulation with photocatalytic activity exceeding that of a commercial photocatalyst by a factor of 1.2 as well as excellent recyclability, with the capability to degrade 3 mg/L methylene blue in aqueous solution over 10 consecutive trials with minimal loss in photocatalytic efficiency. Recovery of the catalyst was achieved by simply exposing the nanocomposite to a magnetic field for ~1 minute. Furthermore, it was found that the catalyst could be regenerated to its initial efficiency through simple UV treatment to provide additional re-use. To highlight the importance of the nanocomposite to the current water treatment industry, we showed rapid degradation of pharmaceutical compounds caffeine and carbamazepine within 60 min. The nanocomposite shows activity exceeding that of commercial photocatalyst P25 with the added benefit of being fully recoverable, reusable, and easy to produce. Overall, a simple technique for producing and tuning an effective magnetically recyclable nanocomposite was developed which should allow easy scalability and industrial production, a factor critical for the implementation of nano-based water treatment techniques.

KEYWORDS: *graphene oxide/reduced graphene oxide, titanium dioxide, photocatalysis, magnetic recovery, recyclability, water treatment*

1. INTRODUCTION

With the emergence of complex organic contaminants resilient to conventional water purification methods, alternative advanced treatment techniques, such as membrane filtration, adsorption, and photocatalysis have come under heavy research.[1−4] Notably, titanium dioxide, a wide band-gap semiconductor with the capability of producing reactive oxygen species in water under UV radiation has proved effective for degrading organic materials, producing benign CO_2 as an end product.[2] This ability to remove contaminants completely and efficiently combined with low cost, low toxicity, and high abundance make it an ideal treatment platform for dealing with organic pollutants.[5,6] However, despite the existence of commercial TiO_2 formulations with excellent photocatalytic efficiency, they have found minimal use in industrial or commercial water treatment. One of the principal reasons for this is the difficulty associated with recovering nano-scale dispersions of the catalyst for re-use, diminishing the potential efficiency of the catalyst and posing an environmental threat due to the release of the catalyst to natural bodies of water.[7,8] Various techniques have been investigated in an attempt to address this issue including immobilization of TiO_2 nanomaterials on various substrates such as sand, glass or polymer beads, membranes, or magnetic nanoparticles.[8−12] While these techniques solve the problems associated with TiO_2 separation after treatment, they simultaneously introduce other problems related to photocatalytic efficiency, such as limiting dispersion of the catalyst throughout the solution thereby limiting interaction with contaminants.[7,13] This can be solved by investigating nanostructured support materials, such as magnetic nanoparticles or graphene oxide (GO) and reduced graphene oxide (rGO), which have been the subject of recent

Received: September 10, 2013
Accepted: March 4, 2014
Published: March 4, 2014

research and retain the ability to effectively disperse in solution.[6,14−20] GO is a robust support structure that is resilient to the oxidative effects of TiO_2 photocatalysis and provides a platform for attaching particles with a high surface area, transparency, and conductivity.[21−24] The electronic properties of GO and rGO have been reported to provide enhancement of TiO_2 photocatalysis by reducing carrier recombination and increasing light absorption range, giving significant advantages to using GO/rGO as support structures.[24,25] Recyclability of such TiO_2 nanocomposites has also been enhanced by depositing magnetic nanoparticles on the same platform. Recently, Tang et al. have produced a magnetically separable nanocomposite consisting of silica insulated Fe_3O_4 particles coated in TiO_2 anchored to a reduced GO sheet.[20] This formulation imparted both magnetic separation capability and superior light harvesting to the photocatalyst. In a similar study, Lin et al. deposited Fe_3O_4 nanoparticles and TiO_2 nanoparticles on rGO to achieve improved separability and light capture over native TiO_2.[26] Additionally, Lin et al. postulated that the rGO support helped mitigate photodissolution that would otherwise occur between TiO_2 and Fe_3O_4 by acting as an electron sink, preventing oxidation of the iron oxide.[26] Both examples demonstrated the capability of the nanocomposite to be recovered and re-used in subsequent trials.[20,26]

Various methods have been reported on the deposition of TiO_2 onto a GO substrate including sol−gel deposition techniques, electrostatic attraction, and thermal or hydrothermal reduction.[16,27] Typically, these deposition techniques involve reaction of precursors to form TiO_2 and magnetic iron oxide particles directly on the surface of the GO support.[28,29] These methods typically require TiO_2 and magnetic particles to be deposited sequentially via a two-step procedure. It is difficult to precisely control the coverage of the GO support by TiO_2 or iron oxide, as well as the reaction parameters for tuning the particle size, rate of reaction, and particle morphology. In this work, we seek to simplify and enhance the production of a magnetically separable TiO_2/GO nanocomposite by using a modular synthesis method in which the ratio of TiO_2 to magnetic particles can be easily tuned. Modular synthesis, in this context, refers to the deliberate arrangement of inorganic components in various combinations to produce materials with selective functionality.[30] This method is anticipated to allow rational optimization of catalysts, particularly inorganic catalysts, for practical applications as illustrated in recent works by Ortel and Milliron.[30,31] In our composites, the magnetic and photocatalytic components can be produced simultaneously and combined in a final step, allowing easy control of composite coverage. The design of this nanocomposite herein employs the use of silica coated controlled aggregates of Fe_3O_4 nanoparticles (SiO_2/CSAs) developed in a previous work. Preventing electronic contact between iron oxide and TiO_2 is essential for preserving photocatalytic efficiency, reusability, and magnetic separability,[32] thus CSAs are coated with SiO_2.[33,34] Compared to using magnetic nanoparticles, the use of CSA particles ensures that sufficient magnetic force for separation is available to each flake of the nanocomposite, allowing quick, efficient recovery. In addition, large magnetic particles will attach to the GO support over a small area compared to individual nanoparticles, leaving many sites open for TiO_2 attachment. The concentration of magnetic particles in the composite can significantly affect its recyclability and separation kinetics, and can be tuned by using a modular synthesis method. By amine functionalizing both these magnetic particles and P25 separately, both particle species can easily be combined in solution with GO at different ratios in a modular fashion to produce tunable nanocomposites. This process allows tuning of both photocatalytic efficiency and magnetic separability simultaneously.

To be impactful on the water treatment industry, the nanocomposite must be efficient in removing contaminants of relevance. Recently, attention has been directed toward the development of novel technologies for removing pharmaceutical compounds from drinking water and wastewater. After digestion and subsequent excretion, pharmaceuticals are released to wastewater as non-metabolized parent compounds or metabolites. These compounds enter surface water as a result of incomplete removal in municipal wastewater treatment plants (WWTPs) and land-based wastewater disposal systems such as septic-systems.[35,36] Pharmaceutical compounds such as caffeine and carbamazepine have become widely distributed in surface water, ground water, and drinking water.[36−40] Alternative treatment methods are required to remove pharmaceutical compounds from both wastewater and drinking water streams.

This study focused on the treatment of caffeine and carbamazepine, two compounds frequently observed in the environment. Caffeine, a popular psychoactive substance, is ingested in beverages, food, and pharmaceutical and personal care products. Although caffeine is biodegradable, it is widely distributed in surface waters and groundwater.[41−43] Carbamazepine, a pharmaceutical compound used to treat epilepsy, bipolar disorder, and trigeminal neuralgia, has been proposed as the tracer of domestic water in the aquatic environment.[44] In contrast to caffeine, carbamazepine is refractory to microbial degradation, and has been reported to be persistent and recalcitrant in the environment as a result of its low biodegradability.[41,45,46] Limited removal of carbamazepine is observed during ozonation treatment, managed aquifer recharge process, granular activated carbon adsorption, and natural photolysis.[47−51] Conkle et al. reported that 51% of input carbamazepine was removed in a lagoon wetland.[52]

Overall, we show that the synthesized nanocomposite can be optimized to give efficient magnetic separation and photocatalytic activity exceeding that of P25, a commercial photocatalyst, by a factor of 1.2. The optimized CSA/TiO_2/rGO also showed capability of being efficiently recovered and reused over 10 water treatment trials and efficacy in degrading the pharmaceutical compounds caffeine and carbamazepine, demonstrating its relevance and usefulness to the current water treatment industry.

2. EXPERIMENTAL SECTION

2.1. Materials. Iron(III) chloride (99%, Sigma) and tetraethyl orthosilicate (TEOS) (99%, Sigma) were purchased as precursors for silica coated CSA synthesis and used without further purification. Sodium citrate dihydrate (99%, Sigma), polyacrylamide (5−6 000 000 MW, Acros), urea (≥99%, Fisher), ammonium hydroxide (28% solution, Sigma), ethanol (EtOH) (99%, ACS), methylene blue (Met-B) (>96%, Sigma), P25 (ACS), (3-aminopropyl)-trimethoxysilane (APTMS) (>95%, Sigma), and graphene oxide (GO) (flakes, Sigma) were purchased and used without further purification.

2.2. Magnetic CSA Synthesis. Controlled aggregates of Fe_3O_4 particles were synthesized according to a method developed previously and modified from Cheng et al.[53−55] Sodium citrate dihydrate (100 mmol/L), urea (105 mmol/L), polyacrylamide (7.5 g/L) and iron(III) chloride (50 mmol/L) were added to 82.5 mL Millipore water. This

solution was stirred to ensure the dissolution of the polyacrylamide. After it was stirred, the solution was transferred to a 125 mL Teflon lined stainless steel autoclave and hydrothermally treated at 200°C for 12 h. The product was washed by magnetic decantation three times with Millipore deionized water followed by three times with EtOH. The product was then dried under flowing nitrogen before being used in the next step.

2.3. Silica Coating of CSAs. Magnetic cores as previously synthesized were coated with a silicon dioxide shell via a Stöber sol-gel reaction. Magnetic cores were added to a solution of EtOH, Millipore deionized water (12 mol/L) and ammonium hydroxide (0.15 mol/L) at a concentration of 1.5 mg/mL such that the final volume was 180 mL. This solution was probe sonicated at 40W for 10 min to ensure good dispersion of particles. The solution was then transferred to an RB flask and stirred mechanically. 1 mol/L TEOS solution in EtOH was added over 1 h so that the final concentration of TEOS in the reaction vessel was 50 mmol/L. The solution was allowed to mix for 18 h overnight before being washed three times with EtOH by magnetic decantation the following day and finally dried under flowing nitrogen before further use (yielding SiO_2/CSAs).

2.4. Amine Functionalization. Amine functionalization was performed on P25 and SiO_2/CSAs separately using a simple APTMS silane coupling reaction. Briefly, particles were dispersed in EtOH at a concentration of 2 mg/mL and probe sonicated at 40 W for 10 min to ensure good dispersion. APTMS was then added so that its concentration in solution was 1% v/v. The solution was then stirred mechanically at 80 °C under reflux for 4 h. After the reaction, the particle solution was washed 3× with EtOH through either magnetic decantation or centrifugation at 4000 rpm.

2.5. Graphene Oxide Addition and Hydrothermal Treatment. Graphene oxide (GO) addition to form the nanocomposite was performed by mixing varying concentrations of amine functionalized particles with GO. GO suspension prepared by sonication of GO flakes at 60 W for 2 h in EtOH, P25 suspension, and SiO_2/CSA suspension were added to EtOH to achieve desired concentrations and a final volume of 100 mL. Particle input masses for tunability studies can be found in Table 1 (section 3.2). After probe sonication at 40 W for 10 min and mechanical mixing for 30 minutes, the solution was magnetically washed three times with DI water, and the solvent replaced by 10 mL of EtOH and 5 mL of Millipore DI water on the final wash. This solution was transferred to a 23 mL PTFE-lined stainless steel reaction vessel and placed in an oven to heat to 180 °C over 1.5 h. The temperature was maintained at 180 °C for 13 h before the final product was recovered and magnetically washed with EtOH 3× before drying under flowing N_2.

Table 1. Synthesis Conditions for Tuning Experiment Nanocomposite Variations

particle weight ratio (TiO_2:SiO_2/CSAs)	mass Of TiO_2 (mg)	mass Of SiO_2/CSAs (mg)	mass Of GO (mg)	GO mass ratio (GO:TiO_2)
1:1	18.75	18.75	1.5	1:12.5
1:4	18.75	75	1.5	1:12.5
1:8	18.75	150	1.5	1:12.5
4:1	75	18.75	1.5	1:50
4:4	75	75	1.5	1:50
4:8	75	150	1.5	1:50
8:1	150	18.75	1.5	1:100
8:4	150	75	1.5	1:100
8:8	150	150	1.5	1:100

2.6. Photocatalytic Removal of Methylene Blue. Photocatalytic reactions for tunability assessment were performed in 50 mL Pyrex beakers. Each beaker contained 40 mL of reaction slurry (5 mg/L methylene blue, 0.1 mg/mL catalyst). The solution was mixed, and then placed under a UV light source (UVP, CL-1000) with maximum output at a wavelength of 254 nm and an intensity of 0.8 W/cm^2. Absorbance of the solution was taken by withdrawing 1 mL aliquots at predetermined time intervals, centrifuging them at 15 000 rpm for 10 min to ensure the absence of nanocomposite, and analysing them using a spectrophotometer (BioTek Epoch Take 3, U.S.A.). Spectrometric measurements were taken at 668 nm as this was found to be the peak absorption wavelength of methylene blue.

For the recyclability study, the reaction slurry was made up using 3 mg/L methylene blue and 0.1 (Met-B) mg/mL catalyst particles. The solution was exposed to UV light, and spectrometric readings were taken as described above after each 30 minute period. At these times, the photocatalyst was magnetically separated from solution and the supernatant was replaced with fresh 3 mg/L Met-B solution and stirred to resuspend settled particles. After 10 consecutive catalysis trials, the nanocomposite were suspended in Millipore water and exposed to a 100 W UV-A light source (UVP Blak-Ray B-100) overnight (16 h exposure). After overnight exposure, the water was replaced with 3 mg/L Met-B solution as described above and catalysis trials resumed. Additionally, recyclability studies were performed using 1 mg/L and 5 mg/L Met-B, and the results of these experiments can be found in the Supporting Information.

2.7. Separation Analysis. Measurement of separation times was performed using 1 mg/mL suspensions of nanocomposite in 20 mL glass vials. Vials were placed in a magnet (LAB 1 × 25 mL, Sepmag) and 1 mL aliquots of the supernatant were drawn every 15 s. After the total 75 s separation time, the aliquots were shaken to ensure good particle dispersion and analyzed by a UV−vis spectrophotometer (BioTek Epoch Take 3, U.S.A.) at 700 nm. The absorbance of the suspension at different times corresponds to the concentration of nanocomposite present at that time.

2.8. Characterization. The size and surface morphology of the particles were analysed with a Philips CM-10 Transmission Electron Microscope (TEM). Samples were prepared by placing 5 μL of aqueous solution containing the photocatalyst on formvar-carbon coated 100 mesh copper TEM grids (Canemco) and allowed to dry overnight in a covered petri dish. XRD data was obtained using a Bruker D8 Advance diffractometer with a $Cu_{K\alpha}$ radiation source (λ = 1.5405 Å) and a Vantec-1 detector. Input voltage and current for XRD measurement were set at 32 kV and 30 mA, respectively. Raman spectroscopy was performed using a Bruker Senterra microscope -spectrometer and data acquisition was done using a wavelength of 532 nm and a power of 0.2 mW. FTIR spectroscopy was done using a Bruker Tensor 27 Fourier Transform Infrared Spectrometer.

2.9. Analytical Procedures for Caffeine and Carbamazepine. Caffeine and carbamazepine were extracted from aqueous solutions using solid-phase extraction (SPE) cartridges, and analyzed using high-performance liquid chromatography (HPLC)-electrospray mass spectrometry. Prior to solid phase extraction, 10 mL samples were spiked with an internal standard mixture containing isotope-labelled caffeine and carbamazepine (Sigma-Aldrich, U.S.A.). Solid-phase extraction was performed using Oasis HLB 3 mL glass cartridges. The cartridges were conditioned with 2 × 1 mL of HPLC grade methanol and then equilibrated with 2 × 1 mL Nanopure water. After loading with 10 mL samples, the cartridges were washed using 2 × 1 mL 5 vol. % methanol, and then eluted with 2 × 1 mL methanol. The eluate was collected in an amber glass vial and stored at 4 °C until analysis. The analytes were separated with an Agilent 1100 HPLC (Agilent Technologies, Mississauga, Canada) and analyzed by electrospray tandem mass spectrometry (MS/MS; 4000 Q TRAP, Applied Biosystems, Foster City, U.S.A.), in positive ESI mode. Analytical procedures were modified slightly from published methods.[56,57] The mobile phase consisted of 0.1% formic acid in nanopure water (phase A) and 100% MeOH with 0.1% formic acid (phase B). The chromatographic separation used a gradient elution which started at 10 % B for 3 min, increased to 90% B over 10 min, and then held at 90% B for 10 min. The separation was achieved in 25 min at a flow rate of 1000 μL min^{-1}. The injection volume was 15 μL. Instrument detection limits for caffeine and carbamazepine were 5.5 and 3.2 ng L^{-1}, whereas method detection limits for caffeine and carbamazepine were 109 and 17 ng L^{-1}.

Scheme 1. Nanocomposite Synthesis Outline[a]

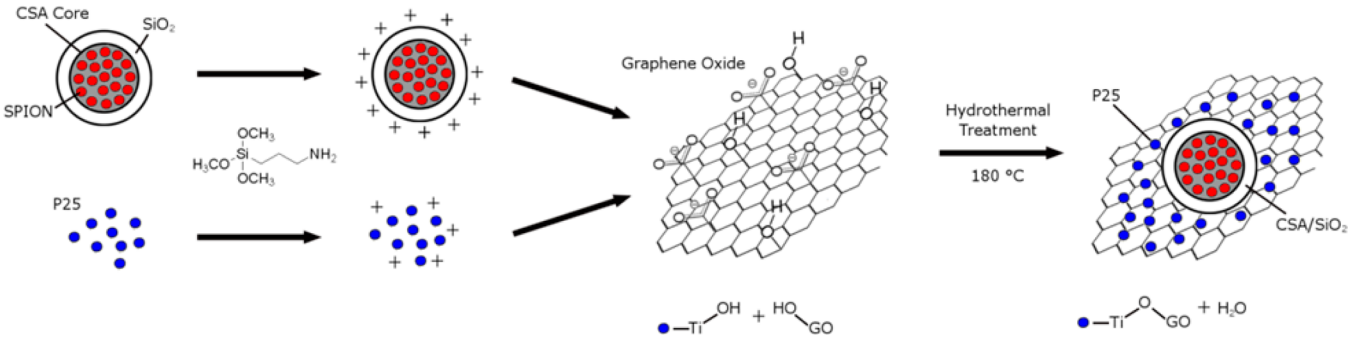

[a]Silica-coated CSAs and P25 are amine functionalized to have a positive surface charge in aqueous solution. The amine functionalized particles are then mixed with GO and electrostatically attracted to the surface of the sheets. The composite then undergoes hydrothermal treatment to reduce the GO and bind the silica coated CSAs and P25 to the rGO.

3. RESULTS AND DISCUSSION

The synthesis of rGO/TiO_2/CSA nanocomposites was designed to provide modular, simple, and tunable control over deposition of the magnetic and TiO_2 particles on the GO sheets. We hypothesized that the GO surface coverage, photocatalytic efficiency and magnetic separability could be tuned by varying the SiO_2/CSA, P25, and GO input, through the synthesis described in Scheme 1.

The first step of synthesis involves the production of silica-coated controlled aggregates of superparamagnetic iron oxide nanoparticles (silica-coated CSA). The synthesis of this core has been detailed in our previous work and is known to retain a superparamagnetic property while providing a high magnetic force per particle. This provides two significant benefits. First, in the absence of an external magnetic field the magnetic particles exhibit no magnetic behavior, preventing aggregation of the nanocomposite.[58,59] Second, after a magnetic field is applied to the particles, they separate quickly because of the large magnetic force imparted by the CSAs. According to the obtained TEM images, the mean diameter of the CSAs is ~354 ±10.7 nm. This diameter increases to 477 ±14.5 nm after silica coating, indicating a silica shell thickness of ~62 nm. Sample TEM images can be found in the Supporting Information. The importance of the silica shell surrounding the magnetic CSA core is related to preserving both photocatalytic efficiency of the nanocomposite and magnetic susceptibility. If TiO_2 and Fe_3O_4 are in direct electronic contact, photodissolution of the Fe_3O_4 can easily occur whereby photogenerated charge carriers produced by TiO_2 could move into Fe_3O_4, diverting them from degrading contaminants and instead dissolving the iron oxide.[32] Use of a silica coating surrounding the Controlled SPION (Superparamagnetic Iron Oxide Nanoparticle) Aggregates (CSA) serves as a barrier to both prevent electronic contact between the Fe_3O_4 and TiO_2,[53] while also shielding the Fe_3O_4 from the highly reactive photocatalytic milieu.

P25 was selected as the TiO_2 source for this nanocomposite for a number of reasons. It is a well known benchmark for photocatalytic activity and also offers an advantage derived from its crystal phase composition, which is approximately 75% anatase and 25% rutile.[60] The resulting heterojunction between the photocatalytically active phases improves separation of photogenerated carriers, improving photocatalytic efficiency.[61] Furthermore, TiO_2 is known to exhibit crystal phase-dependent selectivity in degrading organic compounds, and the efficacy of a TiO_2 photocatalyst toward a specific organic contaminant can be improved by using a nanocomposite of anatase and rutile phases of TiO_2.[60,62,63]

To enable association of the TiO_2 and magnetic particles with the graphene oxide, the surface of CSAs and TiO_2 particles were functionalized with amine groups. This is done through a simple condensation of the silane group of 3-aminopropyl-trimethoxysilane (APTMS) with a surface hydroxyl group of silica or titanium dioxide. This process has been well explored and is known to be compatible with the hydroxylated surface of TiO_2.[64] After both the TiO_2 and SiO_2/CSA particles are amine functionalized, they are mixed with GO in solution at varying ratios. The positively charged amine functionalized surface allows electrostatic interaction of the particles with the negatively charged GO surface.[16] After it is mixed, the nanocomposite is washed to remove weakly-bound particulates, then placed in a hydrothermal vessel. The hydrothermal treatment serves two purposes, the first of which is to link the TiO_2 and SiO_2/CSAs to the GO surface through a condensation reaction. The second function of the hydrothermal treatment is to convert the GO support to reduced graphene oxide (rGO). This improves the electronic properties of the nanocomposite by delocalizing electron density across the support.[65,66] The rGO support structure acts as an electron sink; electrons previously localized in negatively charged functional groups on the GO sheet are distributed and photogenerated electrons can more easily move into the delocalized GO π-bonded network, diminishing carrier recombination within TiO_2, and thereby increasing overall carrier lifetime.[25,66−68] The final nanocomposite consists of TiO_2 particles and insulated magnetic particles randomly distributed across and covalently bonded to the reduced GO surface.

3.1. Surface Characterization of Nanocomposite. The identity of the nanocomposite throughout synthesis was confirmed using FTIR, XRD, and Raman spectroscopy in order to demonstrate the success of amine functionalization, show the crystalline identity of TiO_2 and Fe_3O_4 particles on the nanocomposite, and demonstrate the conversion of the GO support structure to rGO, respectively. Data illustrating the surface properties of the nanocomposite can be seen in Figure 1.

Figure 1A shows FTIR characterization of P25 particles before and after amine functionalization. The peaks appearing at ~2950 cm^{-1} after amine functionalization can be attributed to C−H groups present in the APTMS moiety linked to the

dx.doi.org/10.1021/am4039272 | ACS Appl. Mater. Interfaces 2014, 6, 4658−4668

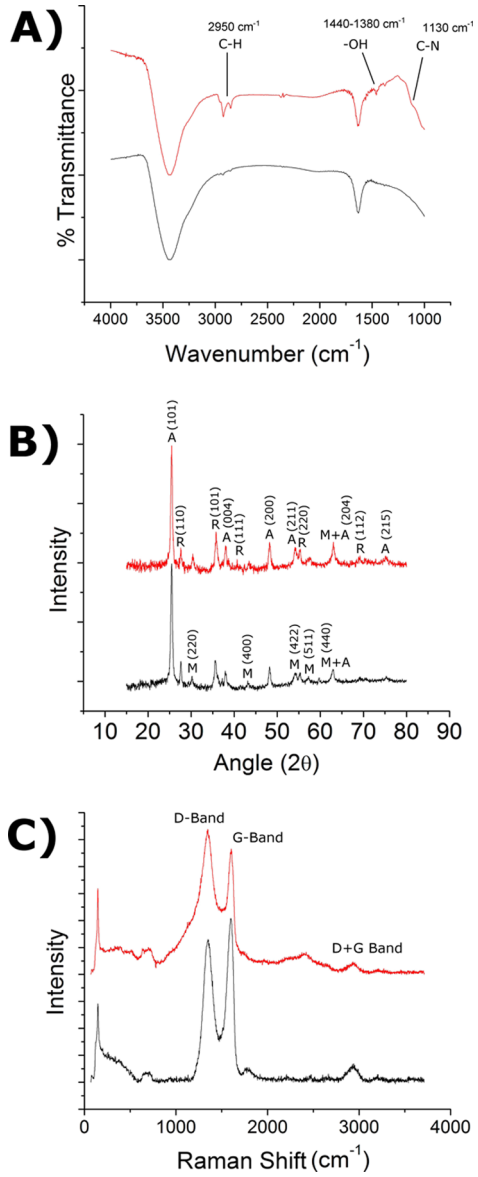

Figure 1. (A) FTIR of P25 particles before (lower) and after (upper) amine functionalization. (B) XRD of nanocomposite before (lower) and after (upper) hydrothermal treatment. Anatase peaks are indicated by an "A" and magnetite peaks by an "M". (C) Raman spectroscopy of nanocomposite before (lower) and after (upper) hydrothermal treatment.

particle surface. The new peaks appearing at ~1440 and ~1380 cm^{-1} are caused by free −OH on unreacted silane groups attached to the APTMS on the surface. Additionally, a low intensity peak visible on the shoulder of the Ti−O−Ti peak at ~1130 cm^{-1} is due to C−N stretching vibrations. This confirms the modification of the surface of the P25 particles by APTMS functionalization.

Figure 1B demonstrates the crystalline phase morphology of the nanocomposite before and after hydrothermal treatment. Hydrothermal processing of TiO_2 is known to affect the crystal structure and is frequently used as a method for crystallizing TiO_2 nanoparticles to anatase. XRD provides confirmation that the crystalline phase of TiO_2 is unaffected by the hydrothermal treatment and is the correct phase composition to provide the nanocomposite with the desired photocatalytic properties. The data in Figure 1B shows that the crystal structure of both magnetite and anatase TiO_2 are preserved through the hydrothermal treatment of the nanocomposite, indicating that both the photocatalytic activity and magnetic separability of the composite should be uncompromised. The peaks labeled "A" are indicative of the anatase TiO_2 crystal phase (JCPDS card # 21-1272), while the 'R' peaks are attributed to the presence of the rutile TiO_2 crystal phase (JCPDS card # 21-1276). Peaks on the lower spectrum labeled "M" are caused by magnetite Fe_3O_4 (JCPDS card # 19-629). All peaks can be observed in both samples, indicating the preservation of crystalline properties throughout hydrothermal treatment.

Finally, Raman spectroscopy confirms the reduction of GO to rGO, and the results can be seen in Figure 1C. Comparing the before and after hydrothermal treatment spectra, there is a significant change in the peak ratio between the D and G bands seen at 1350 cm^{-1} and 1600 cm^{-1}, respectively. This change in intensity ratio is characteristic of a thermal reduction of graphene oxide. As the functional groups leave the GO surface during thermal treatment, the disorder associated with them become more extended and the intensity of the D band with respect to the G band is increased.[66] The sharp peak observable at ~144 cm^{-1} corresponds to a Raman frequency for anatase TiO_2, supporting the crystalline morphology of the TiO_2 present in the sample.[69] The data from Figure 1 supports the synthesis method of the nanocomposite and confirms the identity of the final product in terms of crystalline morphology. The distribution of SiO_2/CSAs and P25 over the nanocomposite can be confirmed via TEM imaging, as seen in Figure 2.

The TEM composite image seen in Figure 2 confirms the structure of the nanocomposite as a random distribution of TiO_2 and SiO_2/CSA particles bound to an rGO sheet. Figure

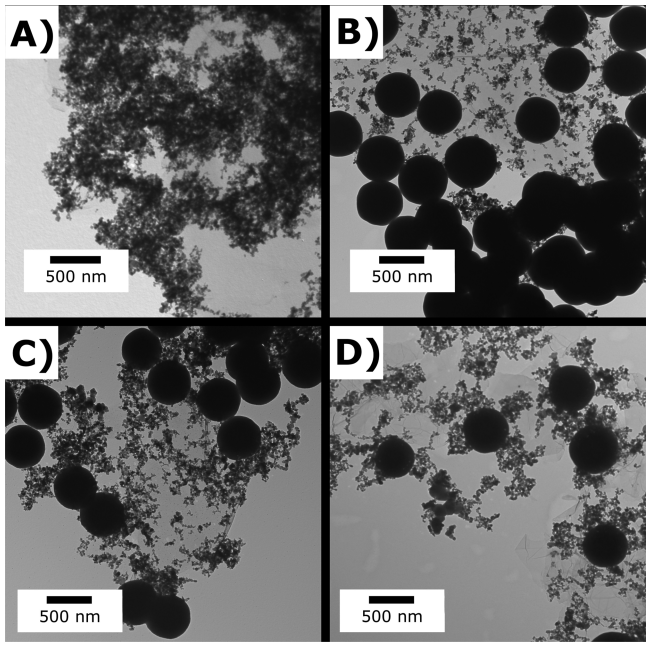

Figure 2. Transmission electron microscopy (TEM) images of the GO/TiO_2/CSA nanocomposite at various particle loadings. All ratios are given as weight ratios. (A) GO loaded with P25 particles (1:100 GO/TiO_2). (B) GO loaded with P25 and silica/CSAs (1:4 P25/CSA, 1:25 GO/TiO_2). (C) GO loaded with P25 and silica/CSAs (1:1 P25/CSA, 1:25 GO/TiO_2). (D) GO loaded with P25 and silica/CSAs (1:1 P25/CSA ratio, 1:12.5 GO/TiO_2.).

dx.doi.org/10.1021/am4039272 | ACS Appl. Mater. Interfaces 2014, 6, 4658−4668

2A–D shows the results of various particle ratios during the GO/P25/CSA mixing step of synthesis. Figure 2A shows TiO_2 loaded onto GO such that the GO is 1% wt. of the TiO_2 mass in the synthesis reaction. Such a high loading concentration gave severe aggregation of the TiO_2 particles and uneven dispersion across the GO surface. Figure 2B demonstrates the effect of reducing the TiO_2 loading by 4 times and introducing SiO_2/CSA particles. By decreasing TiO_2 loading, the TiO_2 particles are much more evenly distributed across the GO flake with decreased aggregation. At a high SiO_2/CSA loading, the same issues as seen with high TiO_2 loading are apparent. An excessive amount of SiO_2/CSA particles are aggregated and poorly distributed across the nanocomposite. Figure 2C shows that SiO_2/CSA distribution can also be improved by reducing synthesis loading concentrations. By decreasing the SiO_2/CSA input by a factor of 4, reduced aggregation and improved particle distribution is achieved. Finally, the effect of GO concentration was also examined. The data from Figure 2 D) shows that by increasing the GO concentration by a factor of 2, both TiO_2 and SiO_2/CSA distribution and aggregation could be improved. Furthermore, the TEM images demonstrate that both TiO_2 and SiO_2/CSA particles are only present in the composite when associated with a GO sheet, evident by the slightly darker background in areas occupied by a GO sheet. This is more evident when a lower magnification image is viewed. The data shown in Figure 2 demonstrates how coverage of the composite can be easily tuned using the modular synthesis technique presented here. Additional TEM micrographs can be found in the Supporting Information.

3.2. Tuning of Photocatalytic Activity and Magnetic Separation. The nanocomposite as shown in Figure 2D was used as a starting point for tuning experimentation. The amount of amine functionalized P25 and SiO_2/CSA particles mixed with GO during synthesis was varied while GO concentration was kept constant. The experiment variations are given in Table 1 and labelled by the ratio of P25 and SiO_2/CSAs relative to the lowest concentrations used.

After synthesis of the different nanocomposites, tests were performed to assess the photocatalytic capabilities of the particles as well as their ability to be quickly magnetically separated. The photocatalytic capability of the particles was measured through a dye degradation assay. The results of these experiments can be seen in Figure 3, in which two trends are examined. The effect of increasing magnetic particle loading while maintaining a constant TiO_2 loading is shown in Figure 3A, and the effect of increasing TiO_2 loading while maintaining a constant SiO_2/CSA loading is demonstrated in Figure 3B. In each case, the amount of TiO_2 added to the photocatalytic test is held constant by varying the amount of nanocomposite added to solution.

Figure 3 shows that at optimal synthesis conditions, the nanocomposite has photocatalytic activity exceeding that of native P25 by a factor of 1.2 when comparing the pseudo-first order rate constants of an exponential fit. This improvement can be attributed to electrostatic interactions between rGO and TiO_2 lengthening the carrier lifetime and favorable adsorption of methylene blue to the rGO surface through $\pi-\pi$ stacking interactions as reported in previous works. Additionally, two trends are seen in Figure 3 that support the ability to tune photocatalytic activity of the nanocomposites through adjustment of synthesis concentrations: as both the amounts of CSA/SiO_2 and TiO_2 particles in the composite are increased, the photocatalytic activity of the composite is decreased. As the

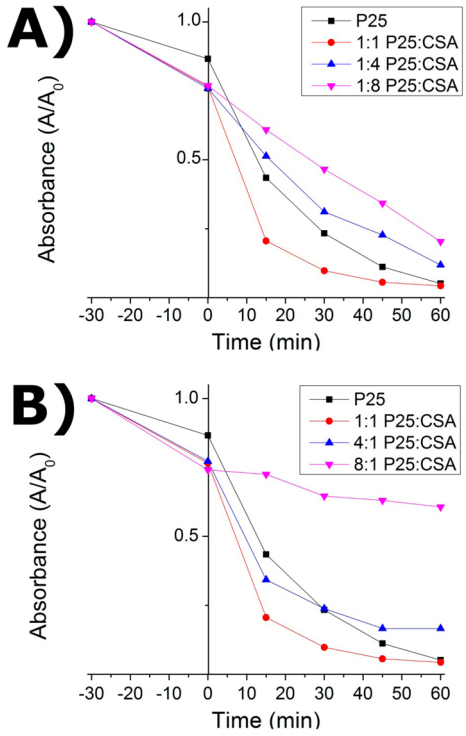

Figure 3. Photocatalytic activity of nanocomposite particle loading variations. Negative time points reflect dark exposure to methylene blue to allow adsorption equilibrium to be reached. (A) Effect of varying CSA loading. (B) Effect of varying P25 loading.

amount of SiO_2/CSA particles in the composite is increased, much of the composite's surface becomes masked by large clusters of this non-photocatalytic particle species as seen in Figure 2B. The diminished activity can be explained by: TiO_2 interaction with the rGO support, contaminant interaction with TiO_2, and light absorption activities on the TiO_2 surface. A number of works have reported synergistic behaviour between TiO_2 and rGO producing longer carrier lifetimes and a wider light absorbance range.[24,25] By saturating surface sites with SiO_2/CSA species instead, this synergistic behaviour is lost and photocatalytic activity is decreased. It is also well established that a critical requirement for efficient photocatalysis is good transfer of the contaminant to the TiO_2 surface.[70] Contaminant species should be held close to active sites to allow short range diffusion of reactive oxygen species.[71] By creating large areas of the composite where TiO_2 is unavailable for reaction, the effective surface area of the material is reduced, affecting activity. Light flux on the TiO_2 surface is also critical to efficient photocatalysis. It has been reported that even too high TiO_2 concentrations in a slurry reactor leads to diminished photoactivity due to reduced radiant flux on the TiO_2 surface.[72] A similar process is occurring here whereby incident light is blocked from reaching TiO_2 by excessive amounts of SiO_2/CSA particles.

The effect of increasing TiO_2 particle loading on the nanocomposite surface was also investigated in Figure 3B and of the loading conditions tested, it was found that a lower TiO_2 particle concentration yielded the best photocatalytic response. This observation matches results seen in recent studies of TiO_2 loading onto graphene oxide where a higher graphene weight percentage elicited superior photocatalytic performance as long as the graphene loading is not excessive enough to interfere with TiO_2 light absorbance.[29] The cause of this trend is likely

dx.doi.org/10.1021/am4039272 | ACS Appl. Mater. Interfaces 2014, 6, 4658–4668

due to reasons similar to those discussed in the effect of SiO_2/CSA loading variation: reduced electrical contact between rGO and TiO_2, reduced contaminant interaction with the catalyst, and decreased light harvesting by the active material. Similar to the CSA loading variations, the amount of TiO_2 in each test was kept at a constant concentration of 0.1 mg/mL. Increasing TiO_2 loading deposits aggregates of TiO_2 particles, as seen in Figure 2A. This limits contact between TiO_2 and rGO and the synergistic effect of these two materials reported previously is less prevalent, reducing activity. Also, by depositing clusters of TiO_2, the contaminant is more likely to interact with the particles on the surface of the cluster, leaving much of the TiO_2 unused during photocatalysis. Furthermore, the TiO_2 accessible to the contaminants would not be in direct contact with rGO, worsening its photocatalytic capability. Finally, any contaminants interacting with TiO_2 within the aggregates would experience further decreased activity due to poor radiant flux on the TiO_2 surface, an important factor in TiO_2 photocatalysis; less light would be accessible to TiO_2 on the inside of aggregate clusters.[72] An additional reason for improved performance at lower TiO_2 loading is access of the contaminant to the rGO surface. The sp^2 hybridized structure of rGO allows preferential adsorption of aromatic or polyaromatic compounds such as Methylene Blue through non-covalent $\pi-\pi$ stacking interactions.[24,73] The adsorption of the dye molecule to the rGO support structure can allow it to be closer to TiO_2, reducing diffusion length for reactive oxygen species and improving photocatalytic efficiency of the nanocomposite.[16,19,20,24] The enhanced adsorption of the dye to rGO can also explain the increased dark adsorption seen in Figure 3 comparative to native P25. Figure 3 indicates that lower TiO_2 and SiO_2/CSA loading produces better efficiency per mass of TiO_2 and that a desirable coverage of both particle species is easily achievable by through modular synthesis.

The effect of magnetic particle loading on separation efficiency of the nanocomposite was also explored as part of the tuning experiments. The magnetic separation efficiency of the particles was assessed by recording the UV−vis absorption of a nanoparticle solution after various separation times. Figure 4 demonstrates the separation times of nanocomposite variations using the maximum TiO_2 loading tested and different loadings of SiO_2/CSA particles.

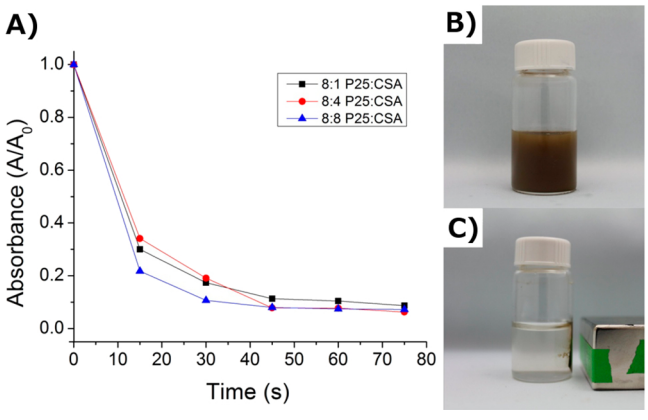

Figure 4. Graph A shows separability of nanocomposite as a function of SiO_2/CSA particle loading. Inset B shows a nanocomposite solution prior to magnetic exposure. Inset C shows the same nanocomposite solution after 1 minute magnetic exposure.

It was found that increasing the loading of SiO_2/CSAs onto the nanocomposite did not have a significant effect on the separation time of the nanocomposite. As seen in Figure 4, after a 75 s separation time, all samples were maximally separated from solution, despite all having the highest TiO_2 loading tested. The nanocomposite solution after only 1 min separation time can be seen in Figure 4 inset B, indicating quick and effective removal of the nanocomposite from aqueous solution. This short separation time is characteristic of CSA particle structure as seen in the literature and our previous works.[6,53,54,58,59] It is likely that the amount of magnetic particles loaded onto the composite, even at the lowest tested synthesis concentrations, provides sufficient magnetic force for separation in a short period of time. Some additional tests were performed using further decreased SiO_2/CSA particle loadings and this data is available in the Supporting Information. At 15:1 and 30:1 P25:SiO_2/CSA synthesis ratios, it was found that the magnetic separability of the nanocomposite was compromised. At such low magnetic particle loadings, the abundance of CSAs is so low that not all GO sheets have an associated magnetic particle and magnetic separation of the nanocomposite is no longer possible. Thus, as long as magnetic particles are suitably abundant, good magnetic separation efficiency and photocatalytic activity for the nanocomposite can be achieved by using a low TiO_2 and magnetic particle loading. This demonstrates the importance of using CSAs as opposed to individual iron oxide nanoparticles as it allows efficient separation to be achieved with minimal surface coverage.

3.3. Magnetic Recyclability of Nanocomposite. The capability of the nanocomposite to be recovered and reused was assessed by performing consecutive photocatalytic degradation reactions using methylene blue as a model contaminant. The most effective nanocomposite sample from previous photocatalytic tests was selected as the candidate for the recyclability study (1:1 P25:CSA). The results of the recyclability study can be seen in Figure 5.

The data shown in Figure 5 conclusively demonstrates the ability of the nanocomposite to be recovered magnetically and

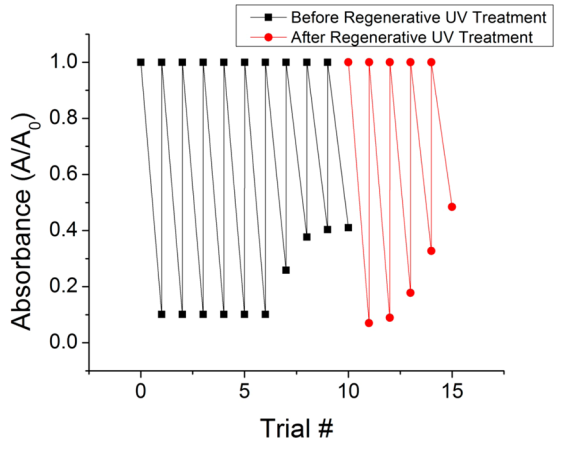

Figure 5. Recyclability study using the 1:1 P25:CSA nanocomposite. Each point at an absorbance of 1 represents replacement of the methylene blue solution. The points represented by the (■) symbol show the consecutive degradation of methylene blue samples over a 5 h period. The points represented by the (●) symbol show the consecutive degradation of methylene blue samples over a 2.5 h period using the same nanocomposite sample after a 16 h treatment by UV-A radiation.

dx.doi.org/10.1021/am4039272 | ACS Appl. Mater. Interfaces 2014, 6, 4658−4668

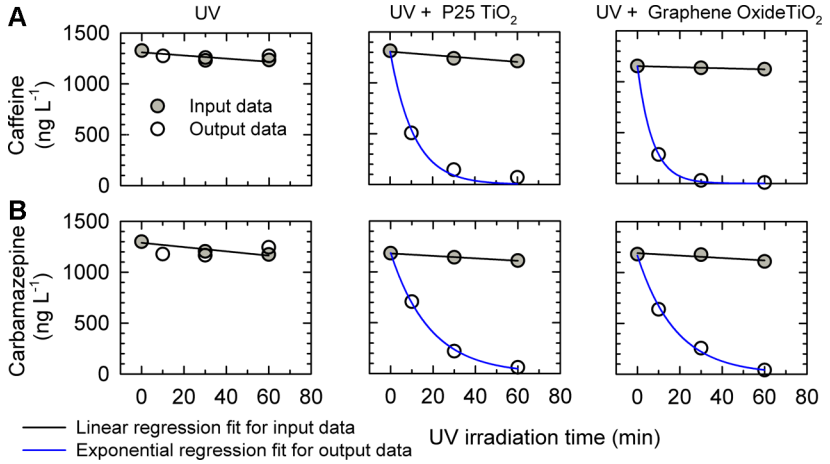

Figure 6. Degradation of caffeine (A) and carbamazepine (B) by P25 and the nanocomposite developed in this work. UV-only treatment shows negligible degradation while the composite matches or exceeds the removal efficiency of P25.

reused in multiple treatments of contaminant solution. Over the first 5 trials, the composite performed without any loss in activity, however in the subsequent 5 trials, the ability of the composite to degrade the model contaminant appeared significantly reduced. It should be noted that the nanocomposite undergoes no washing procedure between degradation trials and is simply stirred with a glass rod to achieve resuspension of the catalyst. This reduction in activity has been seen in previous work and it was found that by suspending the particles in water overnight (16 h) and exposing them to UV-A radition, the activity of the TiO_2 catalyst could be regenerated.[53] The reason for this regeneration effect is due to cleansing active sites on the catalyst surface from unreacted methylene blue or degradation by-products. By exposing the catalyst to UV radiation in water for an extended period of time, any build up of organic contaminant on the surface of the particles is removed by photo-oxidation to smaller compounds and CO_2. This idea that catalytic sites are being occluded by degradation by-products is further supported by results showing that higher concentrations of model contaminant decrease the number of trials at which maximum efficacy is seen. In the Supporting Information, graphs showing the recyclability study using 1 and 5 mg/L methylene blue solutions are available showing a reduced number of trials before activity loss for the higher concentration, and no loss in activity for the lower concentration. The regeneration effect is still evident when testing with a 5 mg/L solution of Methylene Blue indicating that the loss in activity is not due to poor particle recovery. The nanocomposite presented here shows a similar recoverability and reusability to other recent magnetically recoverable TiO_2/rGO composites, but also incorporates a modular synthesis and demonstrates extensive use through regeneration of photocatalytic activity under UV light.[20,26]

3.4. Application to Emerging Contaminants. To highlight the importance and applicability of this nanocomposite to the current water treatment industry, its effect in removing caffeine and carbamazepine from aqueous solution was investigated. Caffeine was selected because of its ubiquity in water and carbamazepine was selected because of its highly recalcitrant nature.[41,45,46] The results of the studies are presented in Figure 6.

The results of photocatalytic treatment of caffeine and carbamazepine showed that <10% of input caffeine and carbamazepine in the control samples were lost during the 60 min treatment test. Caffeine nor carbamazepine was not removed under UV irradiation alone. This resistance of caffeine and carbamazepine to UV photolysis is consistent with other studies.[74,75] Up to 99% of input caffeine and carbamazepine was removed within 60 min UV irradiation with P25 and with graphene TiO_2 (Figure 6).

Langmuir−Hinshelwood (L−H) kinetics model can be used to describe the heterogeneous photocatalysis by TiO_2 particles. The concentrations of caffeine and carbamazepine in this study were low at micrograms per liter; therefore, a pseudo-first-order kinetic equation can be used to simplify the L−H equation.[76] The photocatalytic removal of caffeine and carbamazepine followed a pseudo first order kinetic equation as follows: $c_t = c_0 e^{-kt}$ where k is the pseudo-first-order rate constant (min^{-1}). The first-order rate constants (k) for caffeine and carbamazepine removal during photocatalytic treatment were calculated using SigmaPlot (SPSS Inc.) based on least squares regression (R^2 >0.992).

The concentrations of caffeine decreased from the average input ~1250 ng L^{-1} to less than the method detection limit (109 ng L^{-1}) during the photocatalytic treatment using both P25 and graphene TiO_2 (Figure 6A). The removal rate for caffeine during photocatalytic treatment using P25 was 8.9×10^{-2} min^{-1}, which is lower than the published pseudo first order kinetic rate constant of 12.3×10^{-2} min^{-1};[77] however, caffeine was removed much more rapidly during photocatalytic treatment using graphene oxide TiO_2, with a removal rate of 13.9×10^{-2} min^{-1}. The removal rates for caffeine observed during the photocatalytic treatment using P25 and graphene oxide TiO_2 were at least one order of magnitude more rapid than the rates observed under solar light with TiO_2.[78,79]

The concentrations of carbamazepine decreased from 1180 to 60 ng L^{-1} during the photocatalytic treatment using P25 with a total removal of 95%. More complete carbamazepine removal (97%) was observed during the photocatalytic treatment using graphene oxide TiO_2 (Figure 6 B). The rate of carbamazepine removal was 5.4×10^{-2} min^{-1}during the photocatalytic treatment using P25, and 5.5×10^{-2} min^{-1} using graphene oxide TiO_2. These carbamazepine removal rates are more rapid than observed in previous studies,[74,80,81] but less rapid than observed in other studies.[82]

The laboratory synthesized graphene oxide TiO_2 exhibited catalytic ability comparable or greater than commercial P25 in inducing removal of caffeine and carbamazepine. The enhanced

dx.doi.org/10.1021/am4039272 | ACS Appl. Mater. Interfaces 2014, 6, 4658−4668

catalytic ability of graphene TiO_2 may be attributed to the electronic interactions between rGO and TiO_2 described previously which serve to increase carrier lifetimes through the use of rGO as an electron sink and also a possible widening of the light absorption band.[24,25] Improved removal of caffeine and carbamazepine may also have been affected by improved adsorption of the contaminants to the rGO through $\pi-\pi$ stacking interactions, which has shown to increase photocatalytic performance in other works.[24,73] Using the nanocomposite developed in this work addresses the issue of relevant emerging contaminants by providing a readily separable and reusable TiO_2 material and makes it even more applicable to industry through the use of a modular synthesis technique.

4. CONCLUSIONS

A modular synthesis method allowing for fine tuning of particle coverage and photocatalytic activity of a magnetically recyclable nanocomposite was developed and explored. This method allows for easily scalable production of the material, a factor critical to the implementation of nano-based water treatment techniques. It was found that minimum loading of SiO_2/CSAs and low surface coverage of TiO_2 produced the best activity per mass of TiO_2. At the lowest composite synthesis concentrations tested, the photocatalytic activity of the nanocomposite exceeded that of native P25 by a factor of 1.2 when comparing the pseudo-first order rate constants of an exponential fit. It was also found that at the magnetic particle loadings tested, separation efficiency of the nanocomposite remained relatively unaffected. The ability of the nanocomposite to act as a recyclable catalyst for water purification was assessed through a number of consecutive degradation trials, and the nanocomposite proved capable of successfully treating multiple batches of contaminated water with minimal reduction in photocatalytic efficacy. Furthermore, the activity of the catalyst could be regenerated after multiple trials by simply exposing the nanocomposite to UV radiation for 16 h to clear the surface of adsorbed organic contaminants. Finally, the application of the nanocomposite to real-world water treatment problems was highlighted through the composite's ability to degrade caffeine and carbamazepine, contaminants relevant to industry over 60 min, exceeding the activity of native P25 while also providing easy recovery and reuse. Efficacy on relevant contaminants combined with simple separation after treatment and an efficient, easily controllable modular synthesis technique give the nanocomposite exceptional potential for industrial application of advanced water treatment.

■ ASSOCIATED CONTENT

Ⓢ Supporting Information

Low-magnification TEM imagery of nanocomposite demonstrating particle dispersion, FTIR data supporting amine functionalization of SiO_2/CSAs, photocatalytic data for all permutations given in Table 1, separability data for low CSA synthesis concentrations, and recyclability figures demonstrating catalyst activity using 1 and 5 mg/L methylene blue solution. This information is available free of charge via the internet at http://pubs.acs.org.

■ AUTHOR INFORMATION

Corresponding Author

*Address: Department of Chemical Engineering 200 University Ave. W, Waterloo, ON, N2L3G1, Canada. Tel: (519) 888-4567 ext. 38605. Fax: (519) 888-4347. E-mail: frank.gu@uwaterloo.ca.

Notes

The authors declare no competing financial interest.

■ ACKNOWLEDGMENTS

This work is financially supported by the Natural Sciences and Engineering Research Council of Canada. The authors would like to thank Matthew Gleason, Dennis Liu, and Lori Pollit for their assistance in lab work and characterization for this research.

■ REFERENCES

(1) Prieto-Rodriguez, L.; Miralles-Cuevas, S.; Oller, I.; Agüera, A.; Puma, G. L.; Malato, S. Treatment of emerging contaminants in wastewater treatment plants (WWTP) effluents by solar photocatalysis using low TiO_2 concentrations. *J. Hazard. Mater.* **2012**, *211*, 131−137.
(2) Herrmann, J.-M. Photocatalysis fundamentals revisited to avoid several misconceptions. *Appl. Catal. B* **2010**, *99*, 461−468.
(3) Mills, A.; Davies, R. H.; Worsley, D. Water purification by semiconductor photocatalysis. *Chem. Soc. Rev.* **1993**, *22*, 417.
(4) Pozzo, R. L.; Baltanás, M. A.; Cassano, A. E. Supported titanium oxide as photocatalyst in water decontamination: State of the art. *Catal. Today* **1997**, *39*, 219−231.
(5) Chong, M. N.; Jin, B.; Chow, C. W. K.; Saint, C. Recent developments in photocatalytic water treatment technology: A review. *Water Res.* **2010**, *44*, 2997−3027.
(6) Leshuk, T.; Everett, P.; Krishnakumar, H.; Wong, K.; Linley, S.; Gu, F. Mesoporous magnetically recyclable photocatalysts for water treatment. *J. Nanosci. Nanotechnol.* **2013**, *13*, 3127−3132.
(7) Liu, S.-Q. Magnetic semiconductor nano-photocatalysts for the degradation of organic pollutants. *Environ. Chem. Lett.* **2011**, *10*, 209−216.
(8) Zhao, X.; Lv, L.; Pan, B.; Zhang, W.; Zhang, S.; Zhang, Q. Polymer-supported nanocomposites for environmental application: A review. *Chem. Eng. J.* **2011**, *170*, 381−394.
(9) Qiu, W.; Zheng, Y. A comprehensive assessment of supported titania photocatalysts in a fluidized bed photoreactor: Photocatalytic activity and adherence stability. *Appl. Catal. B* **2007**, *71*, 151−162.
(10) Shen, C.; Wang, Y. J.; Xu, J. H.; Luo, G. S. Facile synthesis and photocatalytic properties of TiO_2 nanoparticles supported on porous glass beads. *Chem. Eng. J.* **2012**, *209*, 478−485.
(11) Zhang, H.; Yang, L. Immobilization of nanoparticle titanium dioxide membrane on polyamide fabric by low temperature hydrothermal method. *Thin Solid Films* **2012**, *520*, 5922−5927.
(12) Watson, S.; Scott, J.; Beydoun, D.; Amal, R. Studies on the Preparation of Magnetic Photocatalysts. *J. Nanopart. Res.* **2005**, *7*, 691−705.
(13) Malato, S.; Fernández-Ibáñez, P.; Maldonado, M. I.; Blanco, J.; Gernjak, W. Decontamination and disinfection of water by solar photocatalysis: Recent overview and trends. *Catal. Today* **2009**, *147*, 1−59.
(14) Liu, Z.; Li, M.; Pu, F.; Ren, J.; Yang, X.; Qu, X. Hierarchical magnetic core−shell nanoarchitectures: non-linker reagent synthetic route and applications in a biomolecule separation system. *J. Mater. Chem.* **2012**, *22*, 2935.
(15) Ao, Y.; Xu, J.; Fu, D.; Shen, X.; Yuan, C. A novel magnetically separable composite photocatalyst: Titania-coated magnetic activated carbon. *Sep. Purif. Technol.* **2008**, *61*, 436−441.
(16) Lee, J. S.; You, K. H.; Park, C. B. Highly photoactive, low bandgap TiO_2 nanoparticles wrapped by graphene. *Adv. Mater.* **2012**, *24*, 1084−1088.
(17) Williams, G.; Seger, B.; Kamat, P. V. TiO_2−graphene nanocomposites. UV-Assisted photocatalytic reduction of graphene oxide. *ACS Nano* **2008**, *2*, 1487−1491.

(18) Zhang, K.; Kemp, K. C.; Chandra, V. Homogeneous anchoring of TiO_2 nanoparticles on graphene sheets for waste water treatment. *Mater. Lett.* **2012**, *81*, 127−130.
(19) Lui, G.; Liao, J.; Duan, A.; Zhang, J.; Fowler, M.; Yu, A. Graphene-wrapped hierarchical TiO_2 nanoflower composite with enhanced photocatalytic performance. *J. Mater. Chem. A* **2014**, in press.
(20) Tang, Y.; Zhang, G.; Liu, C.; Luo, S.; Xu, X.; Chen, L.; Wang, B. Magnetic TiO_2−graphene composite as a high-performance and recyclable platform for efficient photocatalytic removal of herbicides from water. *J. Hazard. Mater.* **2013**, *252-253*, 115−122.
(21) Novoselov, K. S. Electric field effect in atomically thin carbon films. *Science* **2004**, *306*, 666−669.
(22) Lee, C.; Wei, X.; Kysar, J. W.; Hone, J. Measurement of the elastic properties and intrinsic strength of monolayer graphene. *Science* **2008**, *321*, 385−388.
(23) Nair, R. R.; Blake, P.; Grigorenko, A. N.; Novoselov, K. S.; Booth, T. J.; Stauber, T.; Peres, N. M. R.; Geim, A. K. Fine structure constant defines visual transparency of graphene. *Science* **2008**, *320*, 1308−1308.
(24) Zhang, H.; Lv, X.; Li, Y.; Wang, Y.; Li, J. P25-graphene composite as a high performance photocatalyst. *ACS Nano* **2010**, *4*, 380−386.
(25) Du, J.; Lai, X.; Yang, N.; Zhai, J.; Kisailus, D.; Su, F.; Wang, D.; Jiang, L. Hierarchically ordered macro−mesoporous TiO_2−graphene composite films: Improved mass transfer, reduced charge recombination, and their enhanced photocatalytic activities. *ACS Nano* **2011**, *5*, 590−596.
(26) Lin, Y.; Geng, Z.; Cai, H.; Ma, L.; Chen, J.; Zeng, J.; Pan, N.; Wang, X. Ternary graphene−TiO_2−Fe_3O_4 nanocomposite as a recollectable photocatalyst with enhanced durability. *Eur. J. Inorg. Chem.* **2012**, *2012*, 4439−4444.
(27) Lu, J.; Deng, C.; Zhang, X.; Yang, P. Synthesis of Fe_3O_4/graphene/TiO_2 composites for the highly selective enrichment of phosphopeptides from biological samples. *ACS Appl. Mater. Interfaces* **2013**, *5*, 7330−7334.
(28) Liang, Y.; Wang, H.; Sanchez Casalongue, H.; Chen, Z.; Dai, H. TiO_2 nanocrystals grown on graphene as advanced photocatalytic hybrid materials. *Nano Res.* **2010**, *3*, 701−705.
(29) Zhou, K.; Zhu, Y.; Yang, X.; Jiang, X.; Li, C. Preparation of graphene−TiO_2 composites with enhanced photocatalytic activity. *New J. Chem.* **2011**, *35*, 353.
(30) Milliron, D. J.; Buonsanti, R.; Llordes, A.; Helms, B. A. Constructing functional mesostructured materials from colloidal nanocrystal building blocks. *Acc. Chem. Res.* **2014**, *47*, 236−246.
(31) Ortel, E.; Sokolov, S.; Zielke, C.; Lauermann, I.; Selve, S.; Weh, K.; Paul, B.; Polte, J.; Kraehnert, R. Supported mesoporous and hierarchical porous Pd/TiO_2 catalytic coatings with controlled particle size and pore structure. *Chem. Mater.* **2012**, *24*, 3828−3838.
(32) Beydoun, D.; Amal, R.; Low, G. K.-C.; McEvoy, S. Novel photocatalyst: Titania-coated magnetite. Activity and photodissolution. *J. Phys. Chem. B* **2000**, *104*, 4387−4396.
(33) Beydoun, D.; Amal, R.; Low, G.; McEvoy, S. Occurrence and prevention of photodissolution at the phase junction of magnetite and titanium dioxide. *J. Mol. Catal. A* **2002**, *180*, 193−200.
(34) Liu, H.; Jia, Z.; Ji, S.; Zheng, Y.; Li, M.; Yang, H. Synthesis of TiO_2/SiO_2@Fe_3O_4 magnetic microspheres and their properties of photocatalytic degradation dyestuff. *Catal. Today* **2011**, *175*, 293−298.
(35) Bueno, M. J. M.; Gomez, M. J.; Herrera, S.; Hernando, M. D.; Agüera, A.; Fernández-Alba, A. R. Occurrence and persistence of organic emerging contaminants and priority pollutants in five sewage treatment plants of Spain: Two years pilot survey monitoring. *Environ. Poll.* **2012**, *164*, 267−273.
(36) Carrara, C.; Ptacek, C. J.; Robertson, W. D.; Blowes, D. W.; Moncur, M. C.; Sverko, E.; Backus, S. Fate of pharmaceutical and trace organic compounds in three septic system plumes, Ontario, Canada. *Environ. Sci. Technol.* **2008**, *42*, 2805−2811.
(37) Scheurer, M.; Brauch, H.-J.; Lange, F. T. Analysis and occurrence of seven artificial sweeteners in German waste water and surface water and in soil aquifer treatment (SAT). *Anal. Bioanal. Chem.* **2009**, *394*, 1585−1594.
(38) Lapworth, D. J.; Baran, N.; Stuart, M. E.; Ward, R. S. Emerging organic contaminants in groundwater: A review of sources, fate and occurrence. *Environ. Poll.* **2012**, *163*, 287−303.
(39) Kleywegt, S.; Pileggi, V.; Yang, P.; Hao, C.; Zhao, X.; Rocks, C.; Thach, S.; Cheung, P.; Whitehead, B. Pharmaceuticals, hormones and bisphenol A in untreated source and finished drinking water in Ontario, Canada—Occurrence and treatment efficiency. *Sci. Total. Environ.* **2011**, *409*, 1481−1488.
(40) Vulliet, E.; Cren-Olivé, C.; Grenier-Loustalot, M.-F. Occurrence of pharmaceuticals and hormones in drinking water treated from surface waters. *Environ. Chem. Lett.* **2009**, *9*, 103−114.
(41) Benotti, M. J.; Brownawell, B. J. Microbial degradation of pharmaceuticals in estuarine and coastal seawater. *Environ. Poll.* **2009**, *157*, 994−1002.
(42) Kurissery, S.; Kanavillil, N.; Verenitch, S.; Mazumder, A. Caffeine as an anthropogenic marker of domestic waste: A study from Lake Simcoe watershed. *Ecol. Indic.* **2012**, *23*, 501−508.
(43) Seiler, R. L.; Zaugg, S. D.; Thomas, J. M.; Howcroft, D. L. Caffeine and Pharmaceuticals as Indicators of Waste Water Contamination in Wells. *Ground Water* **1999**, *37*, 405−410.
(44) Clara, M.; Strenn, B.; Kreuzinger, N. Carbamazepine as a possible anthropogenic marker in the aquatic environment: investigations on the behaviour of Carbamazepine in wastewater treatment and during groundwater infiltration. *Water Res.* **2004**, *38*, 947−954.
(45) Yamamoto, H.; Nakamura, Y.; Moriguchi, S.; Nakamura, Y.; Honda, Y.; Tamura, I.; Hirata, Y.; Hayashi, A.; Sekizawa, J. Persistence and partitioning of eight selected pharmaceuticals in the aquatic environment: Laboratory photolysis, biodegradation, and sorption experiments. *Water Res.* **2009**, *43*, 351−362.
(46) Zhang, Y.; Geissen, S.-U.; Gal, C. Carbamazepine and diclofenac: Removal in wastewater treatment plants and occurrence in water bodies. *Chemosphere* **2008**, *73*, 1151−1161.
(47) Maeng, S. K.; Sharma, S. K.; Lekkerkerker-Teunissen, K.; Amy, G. L. Occurrence and fate of bulk organic matter and pharmaceutically active compounds in managed aquifer recharge: A review. *Water Res.* **2011**, *45*, 3015−3033.
(48) Patterson, B. M.; Shackleton, M.; Furness, A. J.; Bekele, E.; Pearce, J.; Linge, K. L.; Busetti, F.; Spadek, T.; Toze, S. Behaviour and fate of nine recycled water trace organics during managed aquifer recharge in an aerobic aquifer. *J. Contam. Hydrol.* **2011**, *122*, 53−62.
(49) Grover, D. P.; Zhou, J. L.; Frickers, P. E.; Readman, J. W. Improved removal of estrogenic and pharmaceutical compounds in sewage effluent by full scale granular activated carbon: Impact on receiving river water. *J. Hazard. Mater.* **2011**, *185*, 1005−1011.
(50) Chiron, S.; Minero, C.; Vione, D. Photodegradation processes of the antiepileptic drug carbamazepine, relevant to estuarine waters. *Environ. Sci. Technol.* **2006**, *40*, 5977−5983.
(51) Matamoros, V.; Duhec, A.; Albaigés, J.; Bayona, J. M. Photodegradation of carbamazepine, ibuprofen, ketoprofen and 17α-ethinylestradiol in fresh and seawater. *Water Air Soil Poll.* **2008**, *196*, 161−168.
(52) Conkle, J. L.; White, J. R.; Metcalfe, C. D. Reduction of pharmaceutically active compounds by a lagoon wetland wastewater treatment system in Southeast Louisiana. *Chemosphere* **2008**, *73*, 1741−1748.
(53) Linley, S.; Leshuk, T.; Gu, F. X. Synthesis of magnetic rattle-type nanostructures for use in water treatment. *ACS Appl. Mater. Interfaces* **2013**, *5*, 2540−2548.
(54) Cheng, F. Characterization of aqueous dispersions of Fe_3O_4 nanoparticles and their biomedical applications. *Biomater.* **2005**, *26*, 729−738.
(55) Cheng, W.; Tang, K.; Qi, Y.; Sheng, J.; Liu, Z. One-step synthesis of superparamagnetic monodisperse porous Fe_3O_4 hollow and core-shell spheres. *J. Mater. Chem.* **2010**, *20*, 1799.
(56) Stafiej, A.; Pyrzynska, K.; Regan, F. Determination of anti-inflammatory drugs and estrogens in water by HPLC with UV detection. *J. Sep. Sci.* **2007**, *30*, 985−991.

(57) Vanderford, B. J.; Pearson, R. A.; Rexing, D. J.; Snyder, S. Analysis of endocrine disruptors, pharmaceuticals, and personal care products in water using liquid chromatography/tandem mass spectrometry. A. *Anal. Chem.* **2003**, *75*, 6265−6274.
(58) Sugimoto, T.; Matijević, E. Formation of uniform spherical magnetite particles by crystallization from ferrous hydroxide gels. *J. Colloid Interface Sci.* **1980**, *74*, 227−243.
(59) Cheng, W.; Tang, K.; Sheng, J. Highly Water-soluble superparamagnetic ferrite colloidal spheres with tunable composition and size. *Chem.—Eur. J.* **2010**, *16*, 3608−3612.
(60) Rajeshwar, K.; Osugi, M. E.; Chanmanee, W.; Chenthamarakshan, C. R.; Zanoni, M. V. B.; Kajitvichyanukul, P.; Krishnan-Ayer, R. Heterogeneous photocatalytic treatment of organic dyes in air and aqueous media. *J. Photochem. Photobiol. C* **2008**, *9*, 171−192.
(61) Wang, C.; Zhang, X.; Shao, C.; Zhang, Y.; Yang, J.; Sun, P.; Liu, X.; Liu, H.; Liu, Y.; Xie, T.; Wang, D. Rutile TiO_2 nanowires on anatase TiO_2 nanofibers: A branched heterostructured photocatalysts via interface-assisted fabrication approach. *J. Colloid Interface Sci.* **2011**, *363*, 157−164.
(62) Bui, T. D.; Kimura, A.; Higashida, S.; Ikeda, S.; Matsumura, M. Two routes for mineralizing benzene by TiO_2-photocatalyzed reaction. *Appl. Catal. B* **2011**, *107*, 119−127.
(63) Andronic, L.; Andrasi, D.; Enesca, A.; Visa, M.; Duta, A. The influence of titanium dioxide phase composition on dyes photocatalysis. *J. Sol−Gel Sci. Technol.* **2010**, *58*, 201−208.
(64) Zhao, J.; Milanova, M.; Warmoeskerken, M. M. C. G.; Dutschk, V. Surface modification of TiO_2 nanoparticles with silane coupling agents. *Colloids Surf. A* **2012**, *413*, 273−279.
(65) Morales-Torres, S.; Pastrana-Martínez, L. M.; Figueiredo, J. L.; Faria, J. L.; Silva, A. M. T. Design of graphene-based TiO_2 photocatalysts—A review. *Environ. Sci. Poll. Res.* **2012**, *19*, 3676−3687.
(66) Lim, J.; Choi, K.; Rani, J. R.; Kim, J.-S.; Lee, C.; Hoon Kim, J.; Chan Jun, S. Terahertz, optical, and Raman signatures of monolayer graphene behavior in thermally reduced graphene oxide films. *J. Appl. Phys.* **2013**, *113*, 183502.
(67) Jiang, B.; Tian, C.; Pan, Q.; Jiang, Z.; Wang, J.-Q.; Yan, W.; Fu, H. Enhanced photocatalytic activity and electron transfer mechanisms of graphene/TiO_2 with exposed {001} facets. *J. Phys. Chem. C* **2011**, *115*, 23718−23725.
(68) Du, A.; Ng, Y. H.; Bell, N. J.; Zhu, Z.; Amal, R.; Smith, S. C. Hybrid graphene/titania nanocomposite: interface charge transfer, hole doping, and sensitization for visible light response. *J. Phys. Chem. Lett.* **2011**, *2*, 894−899.
(69) Lottici, P. P.; Bersani, D.; Braghini, M.; Montenero, A. Raman scattering characterization of gel-derived titania glass. *J. Mater. Sci.* **1993**, *28*, 177−183.
(70) Herrmann, J. Heterogeneous photocatalysis: Fundamentals and applications to the removal of various types of aqueous pollutants. *Catal. Today* **1999**, *53*, 115−129.
(71) Chen, X.; Mao, S. S. Titanium dioxide nanomaterials: Synthesis, properties, modifications, and applications. *Chem. Rev.* **2007**, *107*, 2891−2959.
(72) Carp, O. Photoinduced reactivity of titanium dioxide. *Prog. Solid State Chem.* **2004**, *32*, 33−177.
(73) Liu, Z.; Robinson, J. T.; Sun, X.; Dai, H. PEGylated nanographene oxide for delivery of water-insoluble cancer drugs. *J. Am. Chem. Soc.* **2008**, *130*, 10876−10877.
(74) Jelic, A.; Michael, I.; Achilleos, A.; Hapeshi, E.; Lambropoulou, D.; Perez, S.; Petrovic, M.; Fatta-Kassinos, D.; Barcelo, D. Transformation products and reaction pathways of carbamazepine during photocatalytic and sonophotocatalytic treatment. *J. Hazard. Mater.* **2013**, *263* (Pt 1), 177−186.
(75) Shu, Z.; Bolton, J. R.; Belosevic, M.; El Din, M. G. Photodegradation of emerging micropollutants using the medium-pressure UV/H_2O_2 advanced oxidation process. *Water Res.* **2013**, *47*, 2881−2889.
(76) Dimitrakopoulou, D.; Rethemiotaki, I.; Frontistis, Z.; Xekoukoulotakis, N. P.; Venieri, D.; Mantzavinos, D. Degradation, mineralization and antibiotic inactivation of amoxicillin by UV-A/TiO_2 photocatalysis. *J. Environ. Manage.* **2012**, *98*, 168−174.
(77) Marques, R. R. N.; Sampaio, M. J.; Carrapiço, P. M.; Silva, C. G.; Morales-Torres, S.; Dražić, G.; Faria, J. L.; Silva, A. M. T. Photocatalytic degradation of caffeine: Developing solutions for emerging pollutants. *Catal. Today* **2013**, *209*, 108−115.
(78) Alahmad, W.; Alawi, M. Kinetic study of photocatalytic degradation of several pharmaceuticals assisted by SiO_2/TiO_2 catalyst in solar bath system. *Jordan J. Pharm. Sci.* **2010**, *3*, 126−135.
(79) Barndõk, H.; Peláez, M.; Han, C.; Platten, W. E., 3rd; Campo, P.; Hermosilla, D.; Blanco, A.; Dionysiou, D. D. Photocatalytic degradation of contaminants of concern with composite NF−TiO_2 films under visible and solar light. *Environ. Sci. Pollut. Res. Int.* **2013**, *20*, 3582−3591.
(80) Doll, T. E.; Frimmel, F. H. Removal of selected persistent organic pollutants by heterogeneous photocatalysis in water. *Catal. Today* **2005**, *101*, 195−202.
(81) Ziegmann, M.; Frimmel, F. H. Photocatalytic degradation of clofibric acid, carbamazepine and iomeprol using conglomerated TiO_2 and activated carbon in aqueous suspension. *Water Sci. Technol.* **2010**, *61*, 273−281.
(82) Martínez, C.; Canle, L. M.; Fernández, M. I.; Santaballa, J. A.; Faria, J. Kinetics and mechanism of aqueous degradation of carbamazepine by heterogeneous photocatalysis using nanocrystalline TiO_2, ZnO, and multi-walled carbon nanotubes−anatase composites. *Appl. Catal. B* **2011**, *102*, 563−571.